RSC Advances

ROYAL SOCIETY OF CHEMISTRY

www.rsc.org/advances

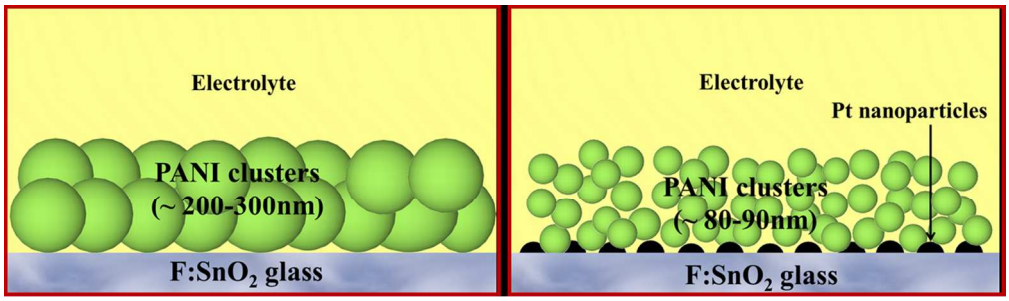

227x66mm (150 x 150 DPI)

Influence of current collector electrode on the capacitive performance of electrodeposited PANI: insight gained from frequency and time domain analysis

Kavita Pandey, Pankaj Yadav, Indrajit Mukhopadhyay[*]

School of Solar Energy, Pandit Deendayal Petroleum University, Gandhinagar- 382007, Gujarat, India

ABSTRACT

This article focuses on the choice and effect of current collector electrode on the performance indicating parameters of supercapacitor. The electrochemical properties of Polyaniline (PANI) deposited on Platinized fluorine doped glass (Pt) and Fluorine doped glass (F:SnO_2) current collectors are evaluated in depth by galvanostatic charge/ discharge (GCD), cyclic voltammetry (CV) and impedance spectroscopy (IS) measurements. The GCD result exhibits that Pt based electrode shows enhanced supercapacitive behaviour than the F:SnO_2 electrode. Scanning electron microscopy (SEM) result reveals that a porous granular array of PANI is induced on Pt electrode whereas a compact granular morphology is induced on F:SnO_2 electrode. The results obtained by CV is used to describe the dynamic variation of capacitance as a function of the applied bias. CV result reveals a higher value of capacitance for Pt based supercapacitor which confirms the higher pore filling by electrolyte ions. The impedance measurement leads to the determination of parameters like equivalent series resistance, rate capability of eletcrodes and AC conductivity of supercapacitors. The results obtained here may lay the basis for understanding that how a simple time and frequency domain experiments can be strategically used for quantative characterization of supercapacitors.

KEYWORDS. Polyaniline (PANI), Cyclic Voltammetry, Impedance Spectroscopy, AC Conductivity

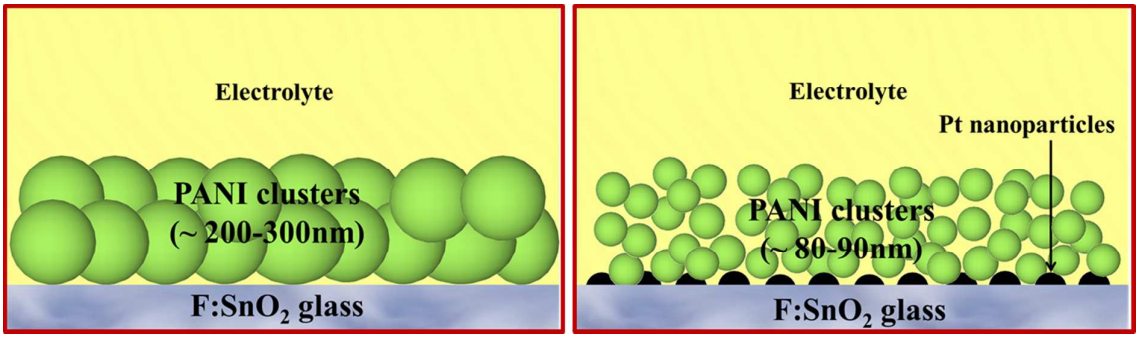

1. INTRODUCTION

The increasing demand of energy and concern about global warming has increased the research interest in the field of energy generation from renewable energy sources.[1,2] However, most of the energy storage devices cannot meet the ever increasing and urgent demand of storing the excess energy generated by renewable sources. Supercapacitors have emerged as a new class of fast energy storage device which can fill the gap between batteries and capacitors.[3,4] Supercapacitors are ideal for applications like portable electronic equipment, hybrid electric vehicle and stand by power system where short term peak power with high power density is required.[5,6] Depending upon the specific capacity and power density, supercapacitors can be classified in several types i.e. (1) Electrochemical double layer capacitors (EDLC's) which works on the mechanism of charge separation at the electrode electrolyte interface with high power density, (2) Pseudo capacitors which works on the mechanism of reversible surface Faradaic redox reaction, with high capacitance and energy density and (3) Hybrid supercapacitors (HSC's) and Asymmetric supercapacitors (ASC's) which works on the principle of redox reaction at one electrode and electric double layer adsorption and desorption on other electrode with high energy and power density.[7,8]

A wide range of metal oxides, conducting polymers and carbonaceous materials are studied and employed for supercapacitor applications.[9] Conducting polymer, Polyaniline (PANI) has attracted considerable attention due to its advantageous properties like environmental stability, low cost, easy doping de-doping, multiple redox states and easy to synthesize in various nanostructures.[10-12] Recently there has been a renewed interest in the synthesis of PANI and its derivative for its potential application in energy storage devices. Mi et al.[13] synthesized nanofiber structured PANI for supercapacitor electrode application, which show a specific capacitance of 428 Fg^{-1} in H_2SO_4 electrolyte. Lie et al.[14] synthesized PANI on titanium substrate which showed a specific capacitance of 837 Fg^{-1} in H_2SO_4 electrolyte. Chen et al.[15] obtained a remarkable energy density of 84 $Whkg^{-1}$ for PANI nanotube grown by utilizing MnO_2 templates. The synthesis of PANI with carbonaceous material like graphene, single wall carbon nanotubes and multiwall carbon nanotubes, various oxides of Ni, Co, In, Sn, Fe, Mn and so forth are also being investigated to develop an economical electrode material with a high capacity for charge storage.[16]

The conventional supercapacitor configuration consist of the following four main sections i.e. electrode, electrolyte, separator and current collector. The heart of the supercapacitor which decides the power delivering rate, efficiency and maximum extraction of stored energy at the electrochemical interface are current collector and morphology of the electrode. The aforementioned parameters are bias, frequency and temperature dependent which provides a critical guidance to determine and optimize the electrode morphology and current collector interface for fabricating and improving the performance of a supercapacitor. The accurate determination of the role of these entities on the performance of a supercapacitor often requires a multiple experimental analysis techniques. Most of the characterization techniques used in this area is simply aimed to measure the overall storage and charge discharge mechanism of a supercapacitor.[17,18] The parameters like transient response, dynamic

behaviour, net terminal impedance and influence of physical parameters on these responses are scarcely discussed in the available literature.

Keeping the above mentioned shortfalls, we have fabricated supercapacitor electrodes with a configuration of Platinized fluorine doped glass substrate/ PANI (Pt/ PANI) and fluorine doped glass substrate/ PANI ($F:SnO_2$/ PANI) while keeping the other mechanistic same for both the electrode. Under these configuration, we have undertaken a detailed study on (1) to determine the limits of traditional techniques (2) a combined use of direct current (DC) and alternating current (AC) technique to explore the voltage and frequency dependent dynamic trend of current collector – electrode interface, where the parallel contribution of the remaining components are described in terms of the established mechanisms.

2. EXPERIMENTAL

Preparation of the electrode. A fluorine doped glass ($F:SnO_2$) and platinized fluorine doped glass (Pt) substrate having 10×10 mm^2 area was purchased from Sigma Aldrich and Dyesol respectively. The use of Platinized $F:SnO_2$ substrate (having a particle size distribution varying from ~25 – 32 nm) was motivated due to its high conductivity, low series resistance and high surface to volume ratio. Aniline purchased from Sigma Aldrich was purified by distillation and stored in a nitrogen glove box prior to use. A monomer solution of aniline in MilliQ water was prepared by using analytical reagent grade hydrochloric acid (HCl). Platinum ring and Ag/ AgCl (saturated KCl) from CH instruments served the purpose of counter and reference electrode respectively. A three electrode cell was used for the electrodeposition of PANI. The cell and counter electrode were cleaned with freshly prepared 1:1 (v/v) H_2O_2/ H_2SO_4 solution followed by ultrasonication in MilliQ water prior to each experiment. All the electrochemical experiments and measurements were performed using potentiostat CH Instruments 660D equipped with a general purpose electrochemical software.

A geometric surface area of 0.7 cm^2 for both the electrodes was exposed to the electrolyte. The monomer solution prepared by using 2% aniline in aqueous 1M HCl (v/v) was used for electropolymerization. Electropolymerization was performed by cycling both the electrodes between -0.2 V to 0.76 V at a sweep rate of 0.015 V/s. The details of the polymerization process of PANI on Highly oriented pyrolytic graphite substrate is discussed in our previous article.[19] After each experiment, the remaining electrolyte was soaked with filter paper and kept for drying. The microstructures of PANI on both the electrodes were produced by terminating the applied potential at initial value. To test the performance of PANI based solid state supercapacitor, approximately 10 wt% Polyvinyl alcohol (PVA) solution in 20 ml deionized water was heated at 75 °C under constant stirring until a clear solution of PVA was obtained. A concentrated solution of H_2SO_4 was added and stirred gently for 45 min to obtain 1:1 PVA-H_2SO_4 solution.

SEM Characterization. Electrodeposited PANI on Pt and F:SnO_2 substrates were placed onto a circular adhesive carbon tape to be affixed to aluminium stubs. The morphology of PANI was investigated using Leo-s 440i scanning electron microscopy with an operating voltage range of 1 – 10 kV under ultra-high vacuum conditions.

Electrochemical Measurements of electrode. All the electrochemical measurements were performed in a two electrode cell where a fine layer of PVA-H_2SO_4 serves as an effective separator. Once the open circuit potential of the system was stabilized, galvanostatic charge/ discharge, cyclic voltammetry (CV) and electrochemical impedance spectroscopy (EIS) were performed in 1M H_2SO_4 aqueous electrolyte. The constant current charge/ discharge cycling was performed at room temperature within the potential window of 0 to 0.65 V with various current densities from 20 μA to 50 μA. The CV data were recorded at different scan rate within the voltage window of 0 to 0.6 V at different scan rate in 1M H_2SO_4 electrolyte.

True analogue ramp mode instead of staircase mode was utilized in all the CV measurements to avoid the problematic transient effect on capacitive current measurements.[20,21] For EIS measurement in H_2SO_4 electrolyte, AC signal of 10 mV amplitude with frequencies between 0.1 Hz and 100 kHz were used. Experimental Nyquist plots were collected at different DC voltages and validated using frequency comparison method where simulations of the impedance behaviour were performed on the basis of equivalent circuit model using a program developed in MATLAB. Unless mentioned otherwise, all the potentials are referred with respect to Ag/ AgCl/ Cl^- (saturated) electrode.

3. RESULTS AND DISCUSSION

Morphological Analysis. The morphology of PANI films on Platinized F:SnO_2 and F:SnO_2 were measured by SEM and is shown in parts A and B of Figure 1 respectively.

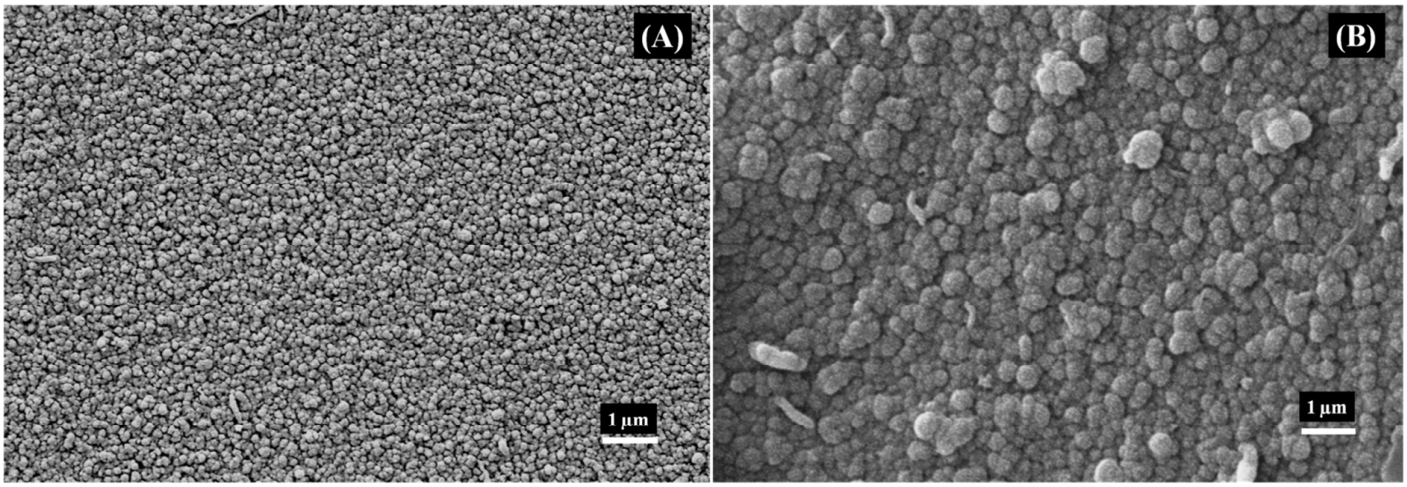

Figure 1. SEM images of (A) Pt/ PANI with 1 µm scale bar and (B) F:SnO_2/ PANI with 1 µm scale bar.

The obtained SEM morphology reveals that the growth of PANI is homogeneous and granular in shape on both the electrodes. The average grain size of PANI on F:SnO_2 and Pt are ~300 nm and ~90 nm, respectively. The approximate distribution and porosity of deposited PANI on both the electrodes is analyzed using ImageJ software and the details are

given in Figure S1 and S2 of ESI†. The porous nanostructure of PANI on Pt has the advantage of providing long and uninterrupted path for electron transport which is favourable for supercapacitor application.[18] A noticeable distribution of large number of grains with almost uniform dimension on F:SnO_2 clearly indicates some chemical as well as electrostatic interaction, which is less prominent in PANI grown over Pt.

From the obtained morphology of PANI over Pt and previously reported results,[20] it is expected that PANI film possesses a higher ionic conductivity and capacitance due to the following reasons: (1) the larger surface area allows higher number of sites for the access of electrolyte. (2) Due to the formation of porous interconnected networks of PANI granules through the entire surface of the film. To confirm these results and to distinguish the contribution from different processes taking place simultaneously, time and frequency response for both the electrodes have been analyzed.

Nucleation and Growth of PANI. Figure 2A and 2B shows the CV recorded during the electropolymerization of PANI with a scan rate of 15 mVs^{-1} in the potential range of - 0.2 to 0.76 V at Pt and F:SnO_2 electrodes respectively. The obtained voltammograms for electropolymerization of PANI are similar to those previously reported by other authors.[22,23] The redox pair i.e. oxidation peak at ~0.23 V and the corresponding reduction peak at ~0.05 V is attributed to the transformation of PANI from the reduced leucoemeraldine state to the partly oxidized emeraldine state.[24]

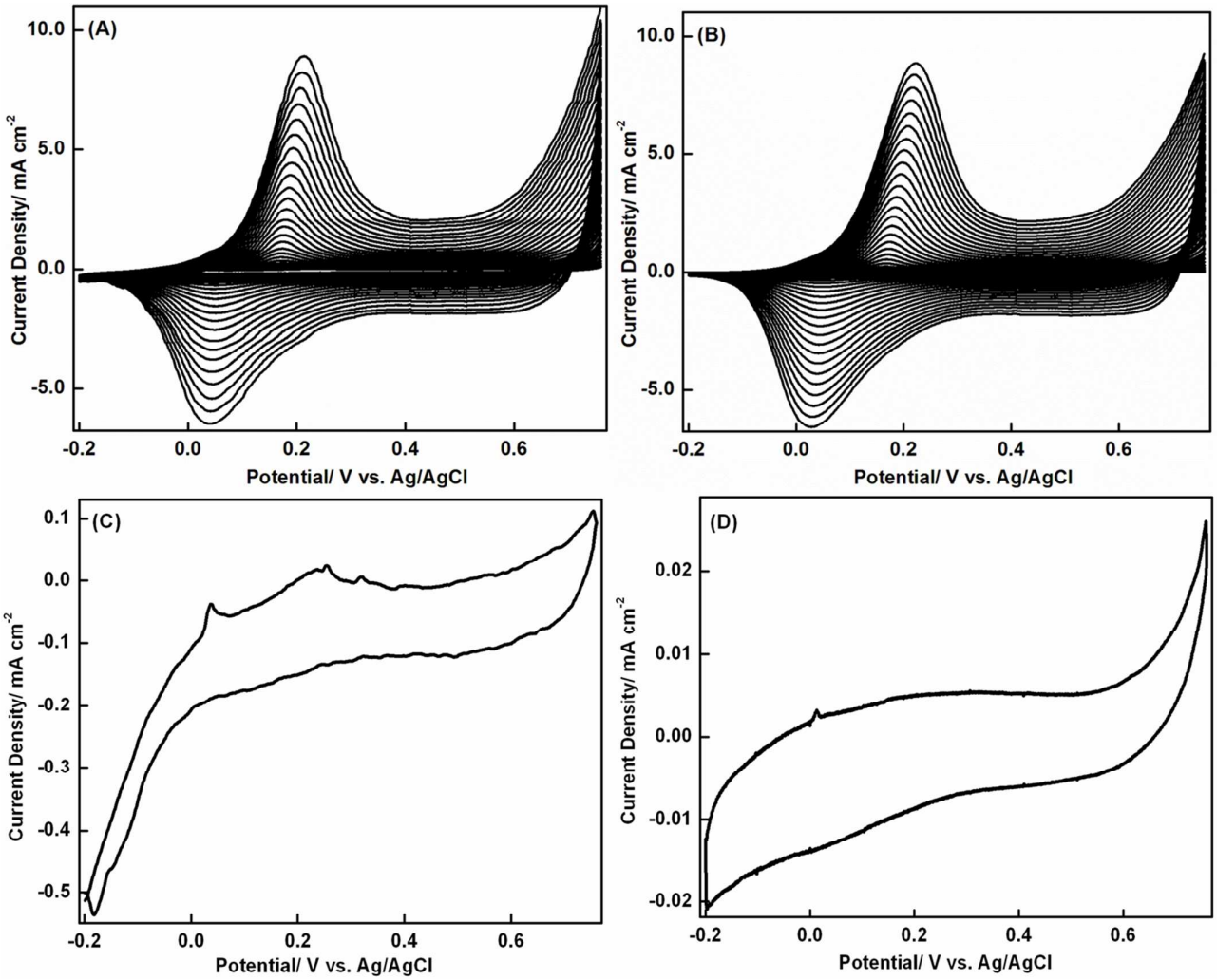

Figure 2. Cyclic voltammograms recorded during electropolymerization of PANI film: (A) on Pt electrode and (B) on F:SnO_2 electrode, First cycle of CV recorded during electropolymerization of PANI film: (C) on Pt electrode and (D) on F:SnO_2 electrode

A weak or almost negligible anodic hump at ~0.5 V indicates an insignificant formation of benzoquinone type degradation product. A rise in current during anodic scan at the terminating potential (~0.76 V) is attributed to the formation of polyemeraldine state of PANI. During the electropolymerization process, the increase in the peak current density with sweep segment is a measure of the growth rate of polymer.[25] To have an insight of different surface morphology (Figure 1) and growth process of PANI at both the electrodes, the first

cycle of CV and total charge under anodic peak as a function of sweep cycle is shown in Figure 2 and Figure S3 of ESI† respectively. The initial cycle of CV at Pt electrode shows a higher current with the electroformation and reduction of leucoemeraldine form of PANI than that of F:SnO_2 electrode. This suggests that due to the electrocatalytic effect of Pt nanoparticles, the growth of PANI on Pt is more favourable than F:SnO_2 electrode. From the charge density plot at lower sweep cycles (inset of Figure S3 ESI†), it is observed that charge density is much low and increases at a very slow rate for F:SnO_2 electrode. This may be because at initial polymerization process the distributed nucleation site causes the development of short chain of PANI nanoparticle whereas after ~12 sweep cycles the charge density for F:SnO_2 electrode increases at a same rate as that of Pt electrode. This leads to the formation of compact layer of PANI or enrichment at local sites. However, in the final polymerization process, the net charge density for Pt and F:SnO_2 electrode are 51 and 49 mC/cm^2 respectively. A small difference in the value of charge density for both the electrodes is due to the higher electroactivity of Pt nanoparticles.

Electrochemical characterization of electrodes: Galvanostatic Charge Discharge. A comparative quasi symmetrical galvanostatic charge discharge plot of F:SnO_2/ PANI and Pt/ PANI electrode within the potential range of 0 to 0.6 V at a constant current of 50 μA/ cm^2 is shown in Figure 3. A deviation in the linearity of charge discharge profile suggests a pseudo capacitive characteristic of both the electrodes. Figure 3 show that the net area under the discharge curve (specific capacitance) for Pt/ PANI electrode is ~30% higher as compared to F:SnO_2/ PANI electrode. In order to get an insight mechanism of higher capacitance obtained for Pt/ PANI electrode, the charge discharge curve is analyzed in two potential regions. The influence of these two potential regions on the performance indicating parameters and its physical origin in supercapacitor will be the subject of discussion in the following sections.

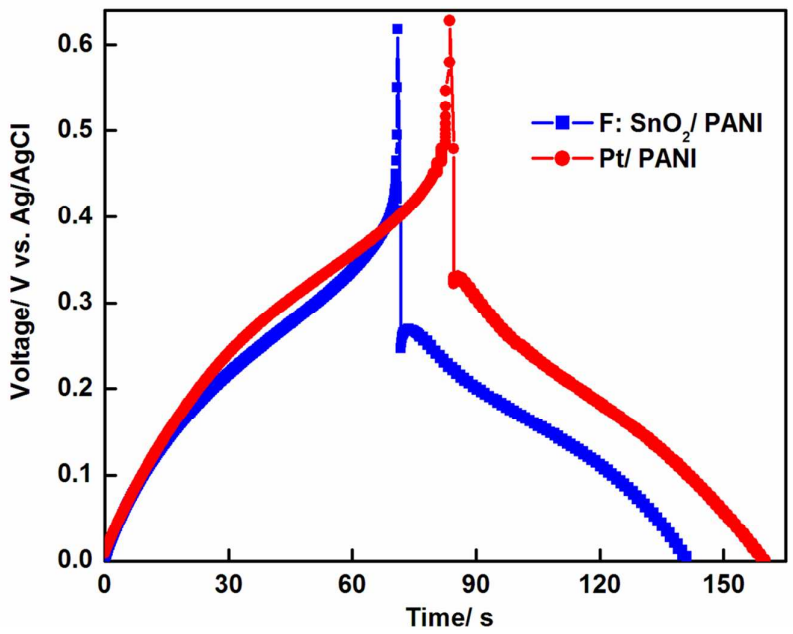

Figure 3. Galvanostatic charge discharge curves of Pt/ PANI and F:SnO_2/ PANI electrodes at a current density of 50 μA/ cm^2

Region I corresponds to the voltage range 0.4 V to 0.6 V where potential drop across internal resistance takes place. Figure 3 shows that in region I (0.4 V to 0.6 V), the internal resistance R_s mainly dominates the discharge curves of both the electrode. The internal resistance is mainly governed by the voltage dependent physical mechanism originated at different layers or interfaces within the supercapacitor. Front contact made of Pt or F:SnO_2, carrier transporting interlayers, charge storing PANI layer and PANI/ electrolyte interface significantly contribute to the value of R_s.[9] The interface formed between active (PANI) layer and front contact mainly dominates the series resistance because of partial energy level alignment, which affects the optimal charge transfer at interface. A comparative examination of region I (Figure 3) for both the electrode, shows that resistive drop (iR_s) associated with F:SnO_2/ PANI (~0.45 V) is more substantial than that of Pt/ PANI (~0.35 V) electrode. The Pt/ PANI electrode offer ~1.5 times lower iR_s drop due to the higher conductivity of Pt

nanoparticle as compared to F:SnO_2 glass which helps in faster charge transfer at the electrode, there by indicating a more proficiency to be used as a supercapacitor electrode.

Region II corresponds to the voltage range 0 V to 0.4 V, where the combined effect of pseudo and electric double layer capacitance dominates the charge discharge profile of the electrode.[26,27] A comparatively longer charge discharge time (Figure 3) obtained for Pt/ PANI electrode signifies a higher value of capacitance than that of F:SnO_2/ PANI electrode. An enhanced electrochemical performance of Pt/ PANI electrode can be attributed to the following reasons i.e. (1) a higher surface area coupled with large number of pores in Pt/ PANI electrode facilitates a deeper penetration of electrolyte ions and a fast electron transfer through the electrode matrix and (2) a higher conductivity of Platinized F:SnO_2 substrate greatly improves the performance of Pt/ PANI electrode by essentially reducing the iR_s drop.

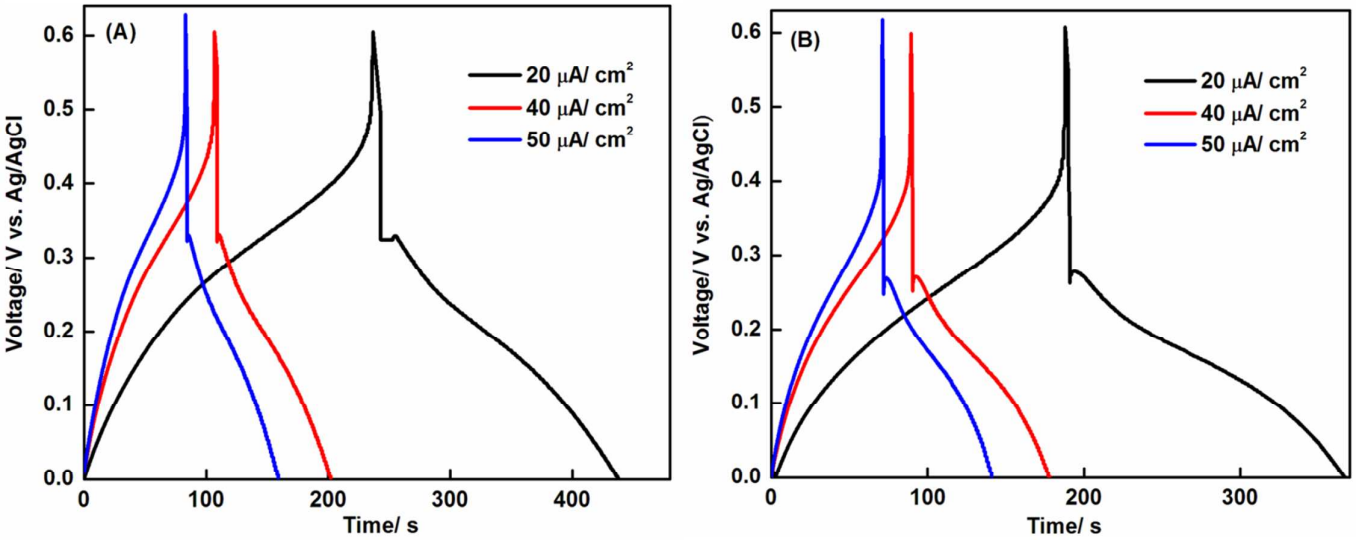

Figure 4. Galvanostatic charge discharge curves of (A) Pt/ PANI and (B) F:SnO_2/ PANI electrodes at different current densities

Figure 4 demonstrates the typical GCD plots of Pt/ PANI and F:SnO_2/ PANI electrode at different current densities. The non-linear charge discharge profiles of both the electrodes deviate from the usual linearity, confirming a redox and pseudo capacitive behaviour of the

electrode. The interfacial capacitance of Pt/ PANI and F:SnO_2/ PANI electrodes were estimated from the slope of discharge curve as $C_A = \frac{I\Delta t}{\Delta V\, S}$ where I is the discharge current, S is the active area of the electrode (cm^2), Δt is the discharge time and ΔV is the voltage window. The calculated interfacial capacitance for both the electrodes at different current density is listed in Table I.

Table I. Electrochemical parameters of Pt/ PANI and F:SnO_2/ PANI

	Discharge current	**F:SnO_2/ PANI**	**Pt/ PANI**
Interfacial Capacitance (mF/ cm^2)	50 µA	5.64	8.94
	40 µA	5.73	8.96
	20 µA	6.76	10.6
Series Resistance (R_s)	-	44.4 Ω	41.9 Ω

Maximum value of interfacial capacitance 10.6 mF and 6.76 mF at 20 µA current density are observed for Pt/ PANI and F:SnO_2/ PANI electrodes respectively. A decrease in the value of interfacial capacitance with an increase in current density is observed for both the electrode signifying the electrode polarization at higher current density and a fast redox kinetic at the electrochemical interface.[8] The obtained results suggest that a comparatively porous architecture of Pt/ PANI facilitates ion diffusion at the electrochemical interface and fast electron collection at current collector which effectively maximizes the capacitance of a supercapacitor. However, the GCD technique is not particularly useful for probing the following parameters of a supercapacitor i.e. (1) transient load for switching application (2) the net terminal impedance and (3) the dynamic trend of interfacial capacitance. A DC (Cyclic voltammetry) and AC characterization techniques (Impedance spectroscopy) are coupled in the same framework of two bias regions (0 to 0.4 V) and (0.4 V to 0.6 V) to get a conclusive evidence about the improved performance and the aforementioned parameters of a supercapacitor.

Scan Rate dependent Cyclic Voltammetry. The analysis of leaky (non – Faradaic) and pseudo (Faradaic) capacitance formed at electrochemical interface from CV at different potential scan rate is straight forward.[28-30] Figure 5 shows the voltammetric response of Pt/ PANI and F:SnO_2/ PANI electrodes in aqueous 1 M H_2SO_4 electrolyte as a function of scan rate within the optimized voltage window of 0 to 0.6 V vs. Ag/ AgCl reference electrode.

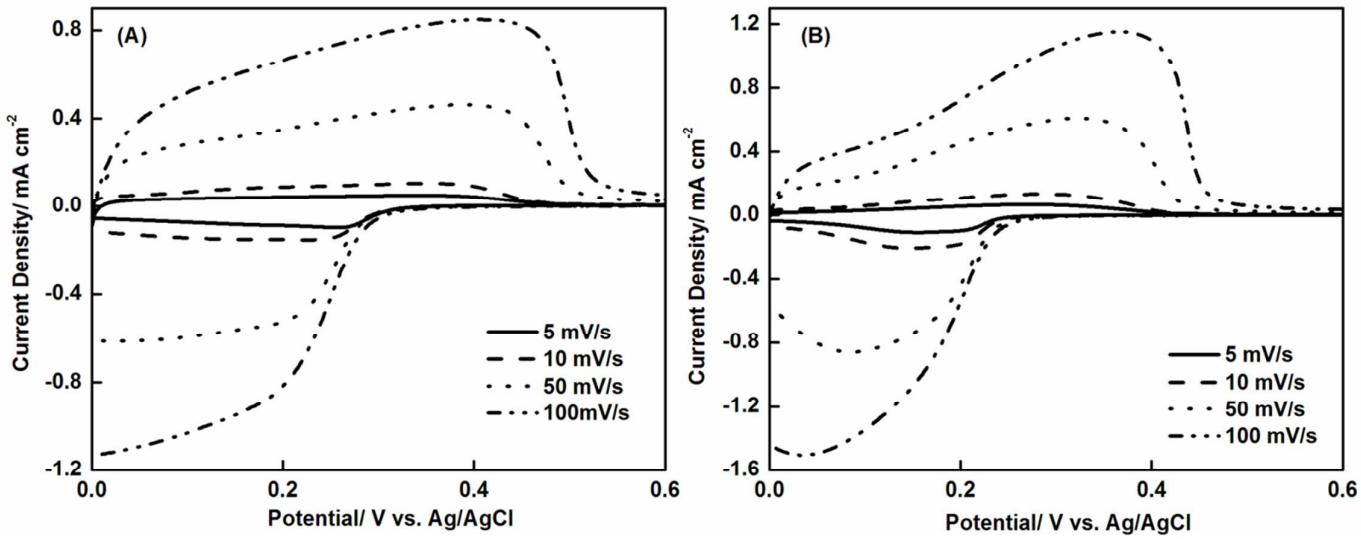

Figure 5. A DC cyclic voltammogram of the interface formed between (A) Pt/ PANI (B) F:SnO_2/ PANI film at different scan rates.

The cyclic voltammogram for both the electrode follows the description of $i = i_r \pm \upsilon_{dc} C_i'$ where i represents the net current, i_r, υ_{dc} and C_i' represents the Faradaic current, scan rate and scaled value of interfacial capacitance respectively.[21,31] The electrochemical response current of the CV curves for both the electrode shows that the positive sweeps are asymmetric to their corresponding counterparts of negative sweeps with reference to zero current line.[9]

A prominent characteristic peak occurring during the positive and negative sweeps of CV for both the electrodes are usually the evidence of pseudo capacitive behaviour and is distinct from the rectangular shape of ideal capacitor with no resistance.[32] A relative comparison of

Figure 5A and 5B shows that a higher Faradaic feature (net area) is observed for Pt/ PANI electrode, which is apparent from the porous nature of PANI over Pt nanoparticles (leading to higher surface area) as compared to the compact nature of PANI over F:SnO_2 glass. A more porous and higher surface area offered by Pt/ PANI film causes an easy insertion and desertion of SO_4^{2-} ions into the polymer matrix leading to a higher electroactivity. Whereas a weak redox activity of F:SnO_2/ PANI is due to the difficulty in exchange and insertion of ions into the compact polymer matrix. A lower value of current in the voltage range of 0.35 - 0.6 V and 0.25 - 0.6 V during the negative sweep for Pt/ PANI and F:SnO_2/ PANI respectively, is originated due to the non-Faradaic feature of electrodes. The current measured within this potential window is mainly governed by charge/ discharge of double layer and are not affected by the Faradaic oxidation or reduction of electrolyte ions. The non-Faradaic feature of both the electrodes in this voltage range causes an iR_s drop in the GCD characteristics.

Furthermore, from Figure 5 it is observed that as scan rate increases, the current under the curve rises successively with a slight change in the CV shape. It can be seen that CV's of both the electrode keep their shape within a selected range of potential even at a high scan rate of 0.2 V/s indicating that PANI films have rapid current response on voltage reversal. Also, a slight shift in the redox peak for both the electrodes with a change in scan rate confirms the active response of Faradaic side reactions.[20,33] For Pt/ PANI electrode, a sharp response of current at each scan rate signifies a good electroactivity and capacitive nature of the electrode. The increase in electroactivity at the film electrolyte interface is mainly attributed to the easy mobility and insertion-desertion of ions through polymer matrix and a higher number of active sites offered by the working electrode. In contrast, CV of previously reported PANI and PANI composite electrodes of similar configurations are different. There are likely to be several reasons for this difference possibly related to the different PANI

morphology and structure, different preparation methods, chemical properties and the substrate.[25,34-36]

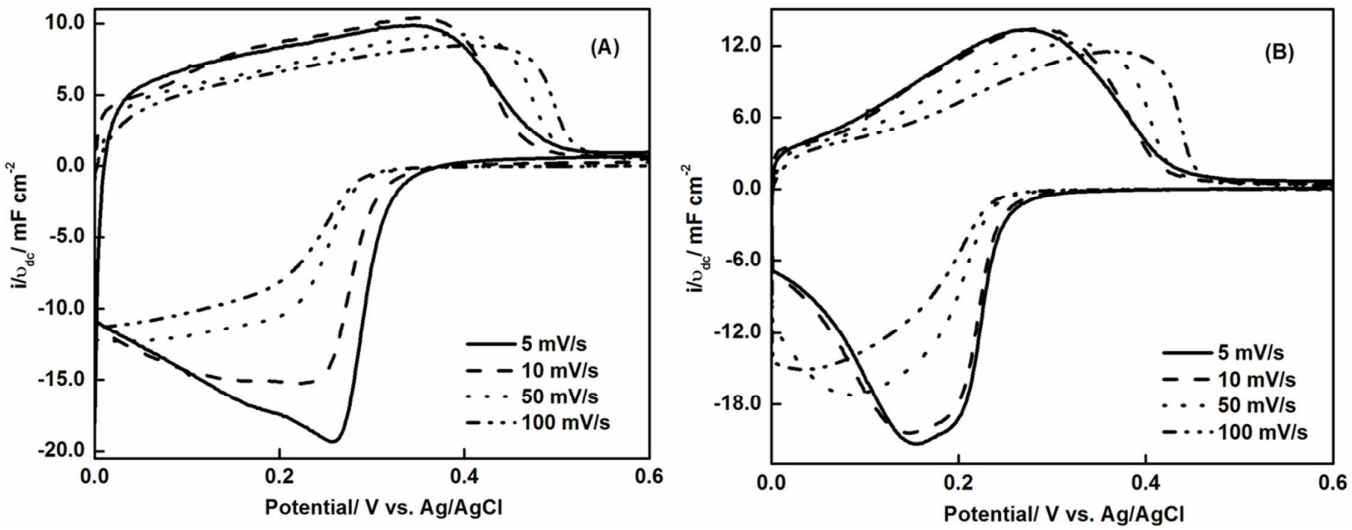

Figure 6. Scan speed normalized electrode current for (A) Pt/ PANI (B) F:SnO_2/ PANI electrodes recorded at different scan rates, recorded with CV.

To have an insight of a linear equation $i = i_r \pm \upsilon_{dc} C_i'$, a scaled version of obtained data from Figure 5 is shown in Figure 6. As the scan rate is increased from 0.005 to 0.1 V/s starting from the outermost to the sequentially underlying plots, the voltammogram gradually reduces on both the sides of zero current axis for both the electrodes.[31,37] This observation is attributed to the presence of inner active sites which cannot precede the redox transitions completely, probably due to the diffusion effect of protons within the electrode. Further reduction in the scan rate will drastically expand the outermost plot by enhancing this effect. The effect of expansion of i/ν_{dc} with the reducing scan rate for both the electrode (Figure 6) cannot be accounted for representing the pseudo capacitance in the present case. This is due to the fact that the evaluation of C_i from CV should be independent of scan rate. Under these circumstances, the interfacial capacitance is calculated by using a linear relation of $\left(C_i =\right.$

$\left(\frac{R_{ct}}{R_s}\right) C_i'$). The polarization resistance R_{ct} from CV and the electrolyte resistance R_s measured by EIS are used to evaluate the value of C_i. The accuracy of the DC measured capacitance depends upon the relative values of R_{ct} and R_s. Figure 7 shows the variation of C_i as a function of applied bias for Pt/ PANI and F:SnO_2/ PANI electrodes. The detailed voltage dependent feature of C_i for both the electrode follows the same trend with a slight deviation in magnitude and bias offset.

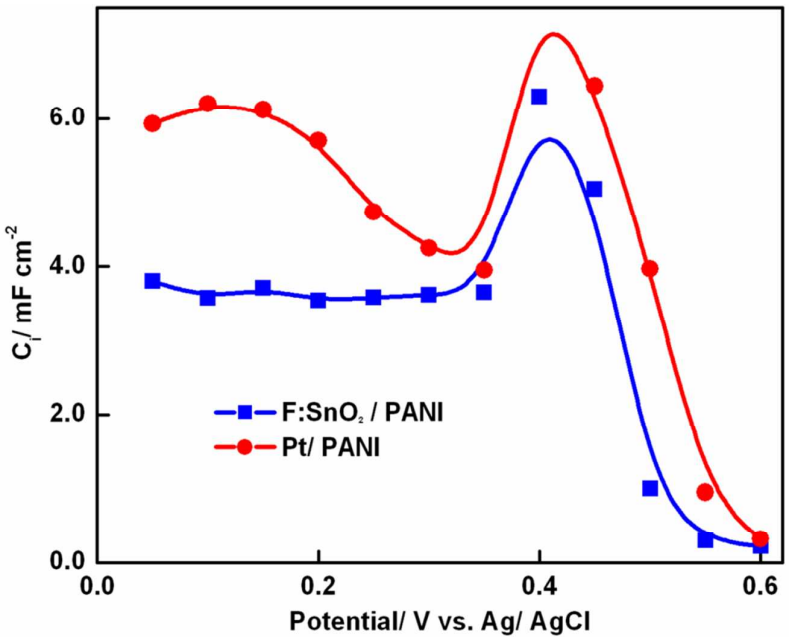

Figure 7. D.C. voltage dependent interfacial capacitance, C_i, obtained for both the electrodes

The observed value of C_i in the bias range (0 to 0.35 V) for both the electrodes are in well agreement with those obtained from GCD measurement and the reason for lower magnitude of C_i for F:SnO_2/ PANI electrode is same as discussed in the explanation of Figure 5. A peak in the bias range (0.35 to 0.55 V) for Pt/ PANI and (0.35 to 0.47 V) for F:SnO_2/ PANI pertain to the conversion of fully oxidized pernigraniline form to emeraldine with the involvement of protons in the redox reaction. Thus, the peak in the value of C_i can be attributed to the following facts: (1) the number of radical cations in the polymer chain is maximized, (2)

increase in the PANI electrolyte real surface which results in enhanced number of available active PANI centres and (3) an increase in the population of quinoidal group inside PANI. The involvement of protons in the redox reaction can be shown as:[38]

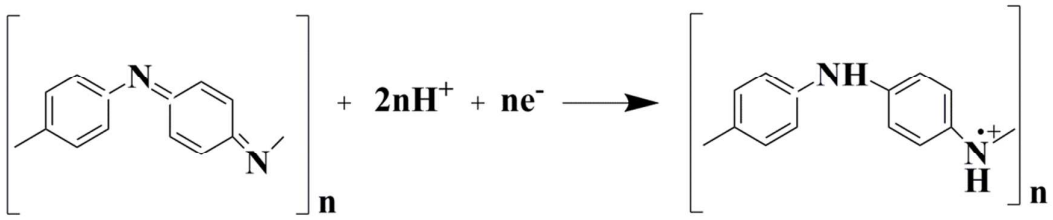

The reduction in the value of C_i at higher bias is due to the fact that the conductivity decreases as the polymer is deprotonated or the oxidation state changes towards either a fully oxidized or a fully reduced state.

The results obtained from DC voltammetry are summarized as follows: (1) a larger value of capacitance is obtained for Pt/ PANI as compared to F:SnO_2/ PANI indicating excessive pore filling and charge transfer taking place at PANI matrix. (2) a sharp drop in the electrode current at higher voltages upon discharge, results from the diffusion limited mobility of electrolyte ions in the electrode pores[39] (3) the capacitance of F:SnO_2/ PANI is pseudo capacitive, mainly arising from the Faradaic reactions of PANI while the capacitance of Pt/ PANI is overwhelmed by the electric double layer capacitance of Pt along with the pseudo capacitance of PANI. In general, a lower internal resistance is required for energy storage devices, so less energy is wasted by producing heat or voltage drop during discharge time.

Electrochemical Impedance Spectroscopy. Electrochemical Impedance Spectroscopy (EIS) has been recognized as one of the principal methods for examining the complex phenomena of electron interception and diffusion at the electrochemical interface.[40-42] An AC response model for elucidating the performance of supercapacitor in frequency domain is shown in the Figure 8, where the DC voltage $'V'$ is combined with frequency dependent

sinusoidal perturbation voltage $'\tilde{V}'$. A Constant phase element (CPE) instead of capacitance is used to account the frequency dispersion effects of AC signal. The CPE is a non – intuitive circuit element to quantify the real world capacitor response and it appears due to the non – uniform distribution of reaction sites at electrode surface.[21,31] The complex impedance of CPE has the form of $Z(C_{dl}) = \frac{1}{Y_0(j\omega)^n}$ where, $j = (-1)^{1/2}$; Y_0 and n are frequency dependent CPE parameters with n in the range of 0 to 1. For $n = 1$, CPE takes the form of capacitance. A Warburg element ($Z_w = w/\sqrt{j\omega}$), to account for the diffusion of ions across the polymer film, is introduced in the mid frequency branch of the equivalent circuit in series with charge transfer resistance R_{ct}, where w is the Warburg coefficient. A parallel combination of interfacial resistance, R_i and C_i is used to account for the Faradaic processes which are responsible for pseudo capacitive behaviour. The various parameters involved in the equivalent circuit can be determined by fitting the net impedance $\left(Z = R_s + \frac{1}{Y_{0_{dl}}(j\omega)^{n_{dl}} + \frac{1}{R_{ct}+Z_W}} + \frac{1}{Y_{0_i}(j\omega)^{n_i} + \frac{1}{R_i}}\right)$ with the obtained experimental EIS data.

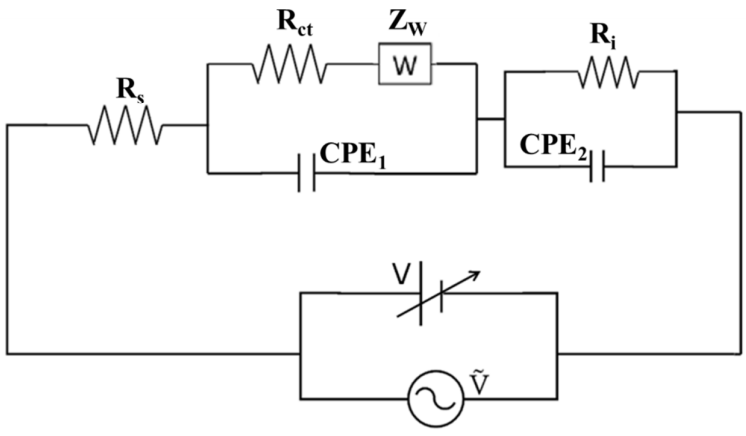

Figure 8. Electrical equivalent circuit employed to fit the impedance spectra obtained at different applied bias for both the electrodes

The EIS data are analyzed using complex Nyquist spectra (also called Cole Cole plot), which represents the frequency response of imaginary and real component of impedance.[43] The maximum and minimum frequency of the impedance spectrum is represented by left most and right most points on each plot respectively. In general, a low frequency perturbation signal requires a relatively longer time for EIS measurement, during which the residual current may modify the electrode surface morphology. Thus, the frequency spectrum of 100 kHz to 0.1 Hz is selected to maintain the validity of EIS measurement in the present study. The parameters selected for analyzing EIS data were optimized through multiple trials to ensure accurate and reproducible result with a mean error of modulus less than 5% indicating that these fitting values are highly accurate. The best values of all parameters for the corresponding equivalent circuits from fitting the EIS data are listed in Table II.

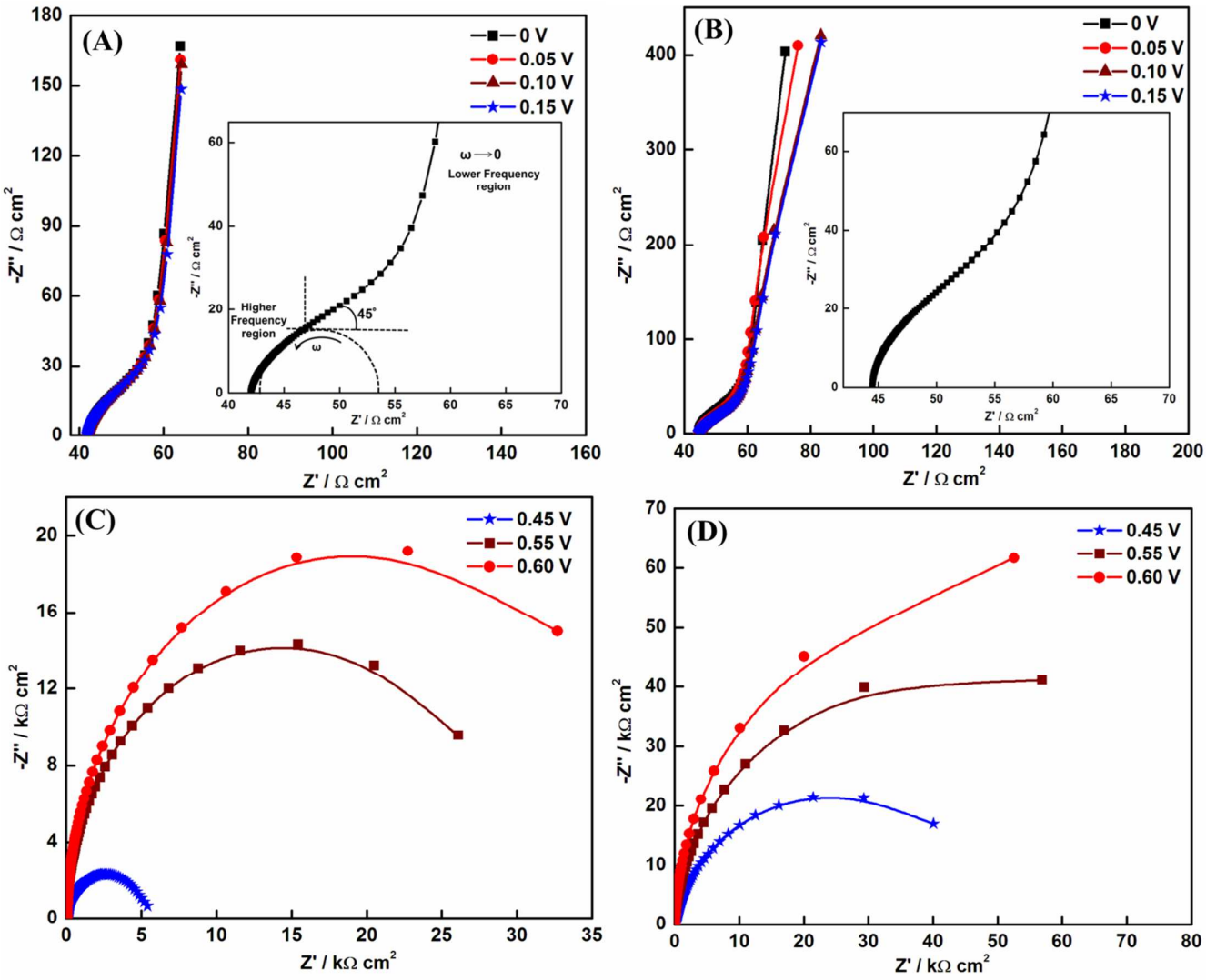

Figure 9. Nyquist plots for (A) Pt/ PANI (B) F:SnO_2/ PANI electrodes in region II. Inset shows the high frequency details of the impedance spectra obtained at 0 bias. Nyquist plots for (C) Pt/ PANI (D) F:SnO_2/ PANI electrodes in region I.

Table II. The best fitting values of the equivalent circuit elements in SI Figure 4 for the impedance data shown in the main article

	Applied Potential (V)	R_s (Ωcm^2)	R_{ct} (Ωcm^2)	Y_{0dl} ($\mu F cm^{-2}$)^{n1}	n_{dl}	W ($\Omega s^{-1/2}$)	R_i (Ωcm^2)	Y_{0i} (mF cm^{-2})^{n2}	n_i	Error (%)
	0	41.1	12.5	48	0.96	208	9	58	0.98	0.7
	0.1	41.1	10.5	44	0.96	185	2000	19	0.99	1.4
	0.2	41.2	10.1	32	0.96	172	4500	70	0.995	0.3
Pt/PANI	0.3	41.2	9.4	20	0.96	172	4580	70	0.995	0.6
	0.4	41.9	30	84	0.82	250	-	-	-	1.2
	0.5	41.8	28000	17	0.83	262	-	-	-	1.9
	0.6	41.8	38000	15	0.86	296	-	-	-	2.2
	0	43.7	24.8	26	1	434	800	20	0.98	0.5
	0.1	43.7	24.1	25	0.96	454	2100	18	0.982	0.9
	0.2	43.7	22	30	0.96	400	4615	18	0.99	1.5
F:SnO_2/PANI	0.3	43.9	20.6	25	0.96	666	4750	6	0.986	1.3
	0.4	44.3	4900	15	0.82	689	-	-	-	1.5
	0.5	44.3	78000	15	0.81	712	-	-	-	2.8
	0.6	44.3	123000	15	0.89	745	-	-	-	1.6

Figure 9 shows that the fitting curve (solid line) and experimental data (symbols) matches well with each other, implying that the equivalent circuit model reflects the electrochemical process occurring at the electrode. The complex Nyquist spectra obtained for both the electrodes features a semicircle in the higher frequency region related to the double layer charging/discharging and R_{ct}. The high frequency semicircle is followed by a 45° segment typified by a Warburg element in the mid frequency region. At very low frequency, a straight line parallel to imaginary axis is accounted by employing R_i and C_i in parallel.[41,44] The point of intersection of real impedance (Z') in the high frequency region represents the equivalent series resistance of the electrode electrolyte interface.

An irregular semicircle at higher frequency can be seen in the inset of Figure 9A and B, due to the irregularity at PANI electrolyte interface. The diameter of the semicircle for Pt/ PANI electrode is smaller than F:SnO_2/ PANI which confirms the result obtained by CV and GCD measurements, that Pt has reduced the value of R_{ct} at current collector. In spite of high conductivity of Pt nanoparticle, another reason for lower R_{ct} of Pt/ PANI electrode is associated with the electropolymerization process during which aniline is oxidized into PANI. During the electropolymerization process, Pt nanoparticles may bind to the available nitrogen sites in a PANI chain and forms an inter chain linkage among several adjacent PANI chains. The reduced R_{ct} of Pt/ PANI electrode leads to the shortening of ion diffusion path which is reflected by an almost vertical line at low frequency, whereas a slight deviation in vertical line is observed for F:SnO_2/ PANI electrode. The fitting results of the elements in equivalent circuit for both the electrodes at open circuit potential can be described as, first series resistance, the value of R_s for Pt/ PANI and F:SnO_2/ PANI is 41.9 Ω and 44.4 Ω respectively. As aforementioned that R_s is mainly contributed from various factors, among which the resistance of the electrolyte solution is predominant.[31,37,43] A lower value of R_s for Pt/ PANI electrode suggests a better charge discharge rate performance as compared to F:SnO_2/ PANI electrode. This fact becomes more prominent by comparing this result with GCD in Figure 3. The second factor is R_{ct}, where the value of R_{ct} for Pt/ PANI and F:SnO_2/ PANI are 12 Ω And 21 Ω respectively. Herein the value of R_{ct} is mainly associated with the dispersion of ions in PANI matrix and the transportation and penetration of ions in the interior of PANI matrix. A lower value of R_{ct} for Pt/ PANI signifies a higher degree of freedom accessed by SO_4^{2-} ions in Pt/ PANI matrix as compared to F:SnO_2/ PANI. The third factor is w, where the value of w for Pt/ PANI and F:SnO_2/ PANI are 210 and 435 $\Omega s^{-1/2}$ respectively. The higher value of w for F:SnO_2/ PANI present the limitation of ion diffusion and indicate that the access of electrolyte ions to the active electrode surface has greater

variation in ion diffusion path length from electrolyte to electrode surface. A similar kind of conclusion has been drawn from the analysis of CV (Figure 5). The fourth factor, C_i, where the value of C_i obtained for Pt/ PANI and F:SnO_2/ PANI are 11 mF/ cm^2 and 4.5 mF/ cm^2 respectively. A lower value of capacitance for F:SnO_2/ PANI are consistent with the explanation of CV.

To get an insight mechanism of iR_s drop in GCD (Figure 3), a complex Nyquist spectra is shown for same bias range (Region I) in Figure 9C and 9D for Pt/ PANI and F:SnO_2/ PANI electrode respectively. From the obtained Nyquist spectra at higher bias and Table II, the value of capacitance becomes almost negligible while the value of resistance dominates the complex Nyquist spectra for both the electrodes. The decrease in conductivity of the polymer due to deprotonation or the change in oxidation state towards either a fully oxidized or a fully reduced state causes a decrease in interfacial capacitance at higher bias. The value of resistance at higher bias is 45 kΩ and 140 kΩ for Pt/ PANI and F:SnO_2/ PANI respectively, signifying a higher iR_s drop for F:SnO_2/ PANI electrode in the discharge characteristics. The above result reveals that the value of R_s, R_{ct}, C_i and w are dependent on the morphology and electrochemical activity of the electrode which are essential for designing the high performing supercapacitor.

The frequency dependence of complex impedance $|Z|$ and capacitance C at different applied potential are shown in Figure 10 and 11 respectively. The $|Z|$ vs. frequency plot in the bias range of 0 to 0.15 V for both the electrodes follows the same trend with difference in their absolute values.

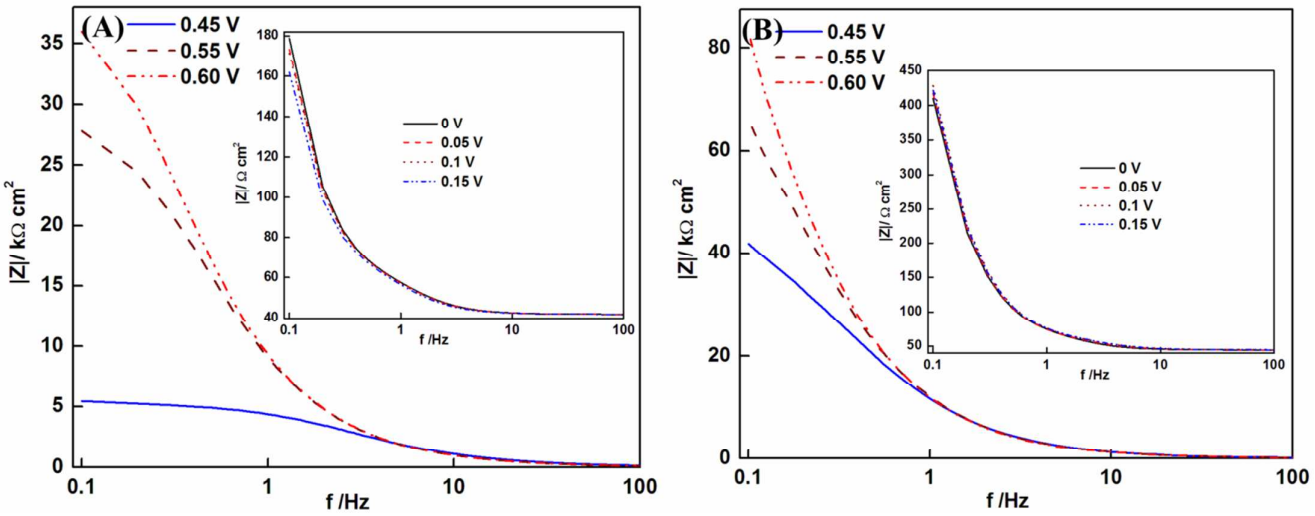

Figure 10. Frequency dependence of magnitude $|Z|$ at different applied potential for (A) Pt/PANI electrode and (B) F:SnO_2/PANI electrode.

The lower value of $|Z|$ for Pt/PANI electrode is again correlated to its lower intrinsic resistance. In the high frequency region, $|Z|$ is weakly dependent on frequency and yields a value of slope very close to zero for both the electrodes which is the characteristic of a pure resistor.[41] However, in the low frequency region a slope of < 1 for both the electrodes signifies the characteristics of a pseudo capacitor. These observations indicate that the behaviour of both the electrode changes from a simple resistor at high frequency to a pseudo capacitor at low frequency. The $|Z|$ vs. frequency plot of both the electrode in the bias region of 0.4 to 0.6 V is essentially different than that of 0 to 0.15 V indicating that the intrinsic charge storage mechanism is qualitatively different in these voltage regions. In the low frequency region $|Z|$ tends to increase with the increase in bias, where the influence of $|Z|$ on the discharge characteristics of supercapacitor is same as those discussed in context of iR_s in the supercapacitor electrode. The value of capacitance at different applied potential as a function of frequency was calculated using the equation $Z^{"} = (2\pi fC)^{-1}$ where $Z^{"}$ is the imaginary part of the impedance, C is the capacitance and f is the frequency.

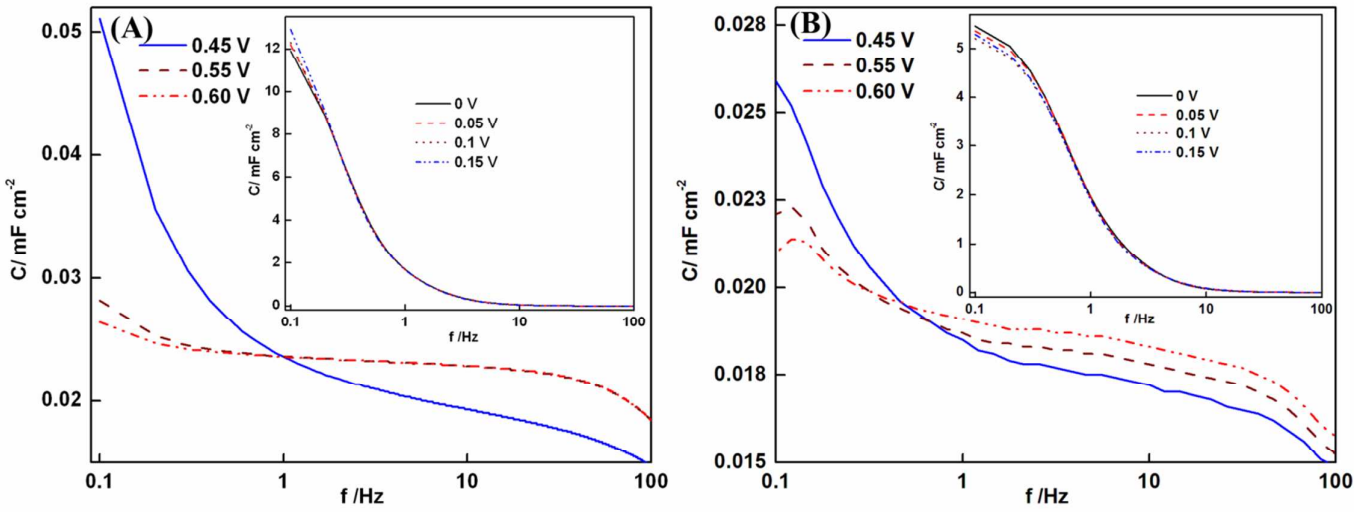

Figure 11. Frequency dependence of capacitance at different applied potential for (A) Pt/PANI electrode and (B) F:SnO_2/PANI electrode.

From the *C* vs. frequency plot, it is observed that the electrode reaches to a full capacitance at low frequency and remains constant at a higher frequency. At low frequency, the value of capacitance for F:SnO_2/PANI electrode tends to saturate whereas a linear trend is observed for Pt/PANI electrode. The value of capacitance obtained from EIS is almost of same order as that obtained from CV at 5 mVs^{-1}. However, the difference in the absolute value of *C* obtained from two different techniques is mainly due to the different response characteristic of electrode to time and frequency domain, amplitude of perturbation signal and number of data sampling per frequency decade.[21,31,37] The *C* vs. frequency plots in the bias range of 0.4 to 0.6 V for both electrode follows the similar behaviour where with the increase in applied bias a decrease in the value of *C* is observed at low frequency.

Electrical property of electrode: AC Conductivity. The charge transport mechanism in the conducting polymer is illuminated by investigating their frequency response. It is often preferable to investigate the frequency dependence of AC conductivity with the charge carrier systems.[8] The AC conductivity (σ_{ac}) of supercapacitor electrodes was calculated from the

impedance data using $\sigma_{ac} = \sigma_{dc} + \omega\, \varepsilon_0\, \varepsilon'\, tan\, \delta$, where σ_{dc}, ω, ε_0, ε' and tan δ are the DC electrical conductivity, angular frequency, permittivity of free space, dielectric permittivity and loss tangent respectively. For insulating materials if $\sigma_{dc} \ll \omega\varepsilon_0\varepsilon' \tan\delta$, then $\sigma_{ac} = \omega\, \varepsilon_0\, \varepsilon'\, tan\, \delta$. However, for conducting polymers σ_{dc} is large and dominates the value of σ_{ac} and hence $\sigma_{ac} = \sigma_{dc}$.

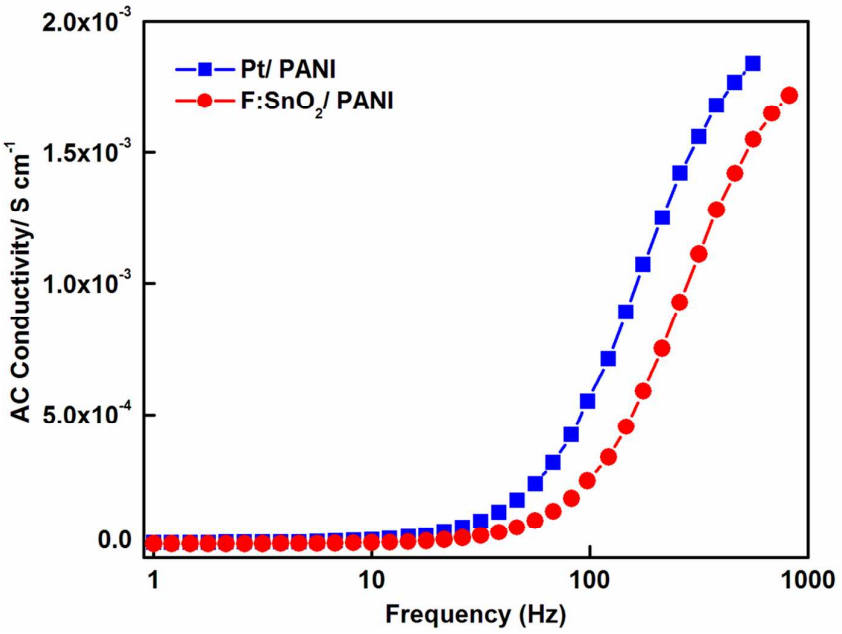

Figure 12. Frequency dependent electrical response of electrodes

The AC electrical conductivity of both the electrodes as a function of applied frequency is shown in Figure 12. The frequency independent plateau appears at low frequency for both the electrodes showing the behaviour of DC conduction. The DC conduction in electrodes arises from the contribution of two components i.e. (1) due to the ionic or electronic conductivity and (2) dielectric factor ($\omega\varepsilon'$) - depend upon the extent of polarization of dipoles and accumulated interfacial charges. At a critical frequency of 60 Hz and 85 Hz for Pt/ PANI and F:SnO_2/ PANI respectively, the plateau response starts to bend upwards and become proportional to the applied frequency. A comparatively higher value of critical frequency (f_c) for F:SnO_2/ PANI electrode signifies that the extra contribution of conductivity comes from

the capacitive region which provides less impedance at higher frequency. The increase in the conductivity at high frequency for both the electrodes can be attributed mainly to the following reason: (1) formation of excess charge carriers, (2) charge moves in the crystalline region and this supports the presence of isolated polarons and bipolarons in this region and (3) the contribution of polarons moving along the shorter distance in the polymer chain.[45]

A lower value of offset in f_c for Pt/ PANI electrode signifies that Pt nanoparticles connect well with the PANI grains and this causes a development of interconnected PANI network with current collector which helps to increase the rate of electron tunnelling pathway. At frequency above f_c, the polarization effect becomes unimportant as the dipoles get insufficient time to align themselves in the direction of applied field. Thus the electric field at $f > f_c$, causes a reduction in space charge accumulation and dispersion of dipoles in field direction that reduces the extent of polarization. This is a necessary phenomenon taking place at Pt/ PANI electrode in terms of constant energy density of supercapacitors. At a f_c of Pt/ PANI, the F:SnO_2/ PANI electrode is still operated in the DC conductivity region where it behaves as a DC blocking capacitor. Thus, the hopping of excited electrons through the PANI layer on Pt becomes easier at a comparatively lower frequency than F:SnO_2/ PANI.

The transient behaviour of supercapacitors are analyzed in terms of complex capacitance analysis (CCA) which has emerged as an excellent technique for investigating the bulk and interfacial electrochemical properties.[46] The capacitive response at low frequency has been widely employed for the study of pseudo capacitors. The imaginary part of complex capacitance $C''(\omega)$ for Pt/ PANI and F:SnO_2/ PANI electrodes as a function of frequency is shown in Figure 13.

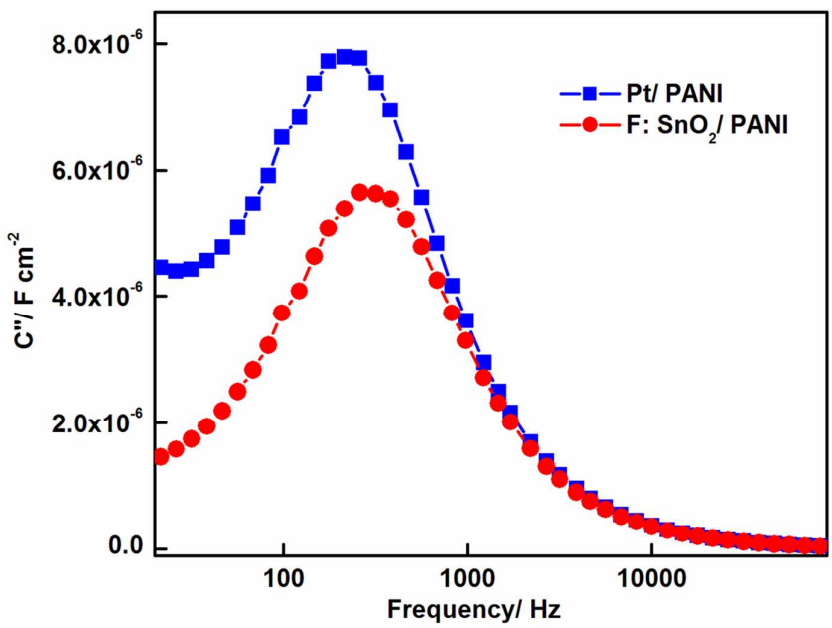

Figure 13. The imaginary part of complex capacitance as a function of frequency

The imaginary part of complex capacitance represents a relaxation process at supercapacitor electrode during the ion transport. The complex capacitance *C"* for both the electrode is extracted from impedance data by using the relation: $C''(\omega) = {Z'(\omega)}/{\omega|Z(\omega)|^2}$ where *Z' (ω)* is the real part of complex impedance *Z (ω)*. The rate capability of an electric system (at which the electrode can discharge) is measured by the value of a characteristic parameter *τ*. The value of τ can be obtained from the peak frequency of the imaginary capacitance plot, by $\tau = {1}/{2\pi f}$.[46] The *τ* measured for Pt/ PANI and F:SnO_2/ PANI are 0.74 μs and 0.61 μs respectively. A smaller value of τ for both the electrodes signifies that a higher output power can be delivered in a short span at output terminal from an electric system. Since time constant reflects the rate capability of the electrode, both the electrode will give poor performance at high charge discharge currents. Thus, although a higher value of capacitance is obtained for Pt/ PANI electrode it has a poor rate capability at high frequency or large charge discharge currents. Therefore it is demonstrated that AC conductivity along with

complex capacitance analysis is able to evaluate the transient behaviour of supercapacitor electrodes which is not possible from the conventional GCD and CV measurements.

CONCLUSION

This article focuses on the choice and effect of current collector electrode on the performance indicating parameters of supercapacitor. The GCD result exhibits that Pt based electrode shows enhanced supercapacitive behaviour than the F:SnO_2 electrode. SEM result reveals that a porous granular array of PANI is induced on Pt electrode whereas a compact granular morphology is induced on F:SnO_2 electrode. The dynamic variation of capacitance with the applied bias reveals that a larger value of capacitance is obtained for Pt/ PANI as compared to F:SnO_2/ PANI indicating excessive pore filling and charge transfer taking place at PANI matrix. The sharp drop in the initial voltage upon discharge results from the diffusion limited mobility of electrolyte ions in the electrode pores and the capacitance of F:SnO_2/ PANI mainly arises from the Faradaic reactions of PANI while the capacitance of Pt/ PANI is overwhelmed by the electric double layer capacitance of Pt along with the pseudo capacitance of PANI. The impedance measurement leads to the determination of parameters like equivalent series resistance, rate capability of eletcrodes and AC conductivity of supercapacitors.

AUTHOR INFORMATION

Corresponding Author

School of Solar Energy, Pandit Deendayal Petroleum University, Gandhinagar- 382007, Gujarat, India

Tel.: +91 – 9586864936, Fax. +91-79-23275030

E-mail address: indrajit.m@sse.pdpu.ac.in (Indrajit Mukhopadhyay)

ACKNOWLEDGEMENT

The authors gratefully acknowledge Dr. Narendra Chauhan, FCIPT, IPR, for the SEM measurements and DST (Project No. SR/S1/PC-44/2011 dated 04/07/2012) for the financial assistance. One of the author (K.P.) thanks DST INSPIRE fellowship program for junior research fellowship.

REFERENCES

1. M. K. Deshmukh and S. S. Deshmukh, *Renew. Sust. Energ. Rev.,* 2008, **12**, 235.
2. J. E. Garland, D. J. Crain, J. P. Zheng, C. M. Sulyma and D. Roy, *Energy Environ. Sci.*, 2011, **4**, 485.
3. L. F. Chen, X. D. Zhang, H. W. Liang, M. Kong, Q. F. Guan, P. Chen, Z. Y. Wu and S. H. Yu, *ACS Nano,* 2012, **6**, 7092.
4. W. Liu, X. Yan, J. Lang, J. Pu and Q. Xue, *New J. Chem.,* 2013, **37**, 2186.
5. Y. Zhai, Y. Dou, D. Zhao, P. F. Fulvio, R. T. Mayes and S. Dai, *Adv. Mater.,* 2011, **23**, 4828–4850.
6. F. Su, C. K. Poh, J. S. Chen, G. Xu, D. Wang, Q. Li, J. Lin and X. W. Lou, *Energy Environ. Sci.*, 2011, **4**, 717.
7. F. Wang, S. Xiao, Y. Hou, C. Hu, L. Liu and Y. Wu, *RSC Adv.* 2013, **3**, 13059.
8. S. Maiti and B. B. Khatua, *RSC Adv.,* 2013, **3**, 12874.
9. S. B. Kulkarni, U. M. Patil, I. Shackery, J. S. Sohn, S. Lee, B. Park and S. Jun, *J. Mater. Chem. A*, 2014, **2**, 4989.
10. I. Kovalenko, D. G. Bucknall and G. Yushin, *Adv. Funct. Mater.,* 2010, **20**, 3979.
11. L. Shao, J. W. Jeonand and J. L. Lutkenhaus, *J. Mater. Chem. A*, 2014, **2**, 14421.
12. K. Xu, W. Lin, M. Xin, J. Peng, Y. Xing and M. Chen, ***RSC Adv.***, 2014, DOI: 10.1039/C4RA04422C.

13. H. Mi, X. Zhang, S. Yang, X. Ye and J. Luo, *Mater. Chem. Phys.,* 2008, **112**, 127.

14. G. R. Li, Z. P. Feng, J. H. Zhong, Z. L. Wang and Y. X. Tong, *Macromolecules,* 2010, **43**, 2178.

15. W. Chen, R. B. Rakhi and H. N. Alshareef, *J. Mater. Chem. A,* 2013, **1**, 3315.

16. S. Xiong, J. Wei, P. Jia, L. Yang, J. Ma and X. Lu, *ACS Appl. Mater. Interfaces*, 2011, **3**, 782.

17. H. Gao, F. Xiao, C. B. Ching and H. Duan, *ACS Appl. Mater. Interfaces*, 2012, **4**, 2801.

18. X. Chen, H. Wang, H. Yi, X. Wang, X. Yan and Z. Guo, *J. Phys. Chem. C*, 2014, **118 (16)**, 8262.

19. D. Bhattacharjya and I. Mukhopadhyay, *Langmuir*, 2012, **28**, 5893.

20. K. Pandey, P. Yadav and I. Mukhopadhyay, *J. Phys. Chem. B*, 2014, **118 (11)**, 3235.

21. J. P. Zheng, C. M. Pettit, P. C. Goonetilleke, G. M. Zenger, and D. Roy, *Talanta*, 2009, **78**, 1056.

22. W. C. Chen, T. C. Wen and A. Gopalan, *Synth. Met.,* 2002, **128**, 179.

23. W. C. Chen, T. C. Wen, C. C. Hu and A. Gopalan, *Electrochim. Acta*, 2002, **47**, 1305.

24. Z. Tang, J. Wu, M. Zheng, Q. Tang, Q. Liu, J. Lin and J. Wang, *RSC Adv.*, 2012, **2**, 4062.

25. M. H. Pournaghi-Azar and B. Habibi, *Electrochim. Acta*, 2007, **52**, 4222.

26. W. Fan, C. Zhang, W. W. Tjiu, K. P. Pramoda, C. He, T. Liu, *ACS Appl. Mater. Interfaces,* 2013, **5**, 3382.

27. J. Zhang and X. S. Zhao, *J. Phys. Chem. C*, 2012, **116**, 5420.

28. J. P. Zheng, P. C. Goonetilleke, C. M. Pettit and D. Roy, *Talanta,* 2010, **81**, 1045.

29. X. Wen, D. Zhang, T. Yan, J. Zhang and L. Shi, *J. Mater. Chem. A, 2013, **1**,* 1233.

30. H. Wang, L. Shi, T. Yan, J. Zhang, Q. Zhonga and D. Zhang, *J. Mater. Chem. A*, 2014, **2**, 4739.

31. J. Zheng, S. S. Moganty, P. C. Goonetilleke, R. E. Baltus and D. Roy, *J. Phys. Chem. C*, 2011, **115**, 7527.

32. Y. Li, X. Zhao, Q. Xu, Q. Zhang and D. Chen, *Langmuir*, 2011, **27**, 6458.

33. L. Bertoluzzi, I. Herraiz-Cardona, R. Gottesman, A. Zaban and Juan Bisquert, *J. Phys. Chem. Lett.*, 2014, **5**, 689.

34. V. Gupta and N. Miura, *Mater. Lett.,* 2006, **60**, 1466.

35. V. Gupta and N. Miura, *Electrochim. Acta*, 2006, **52**, 1721.

36. H. Li, J. Wang, Q. Chu, Z. Wang, F. Zhang and S. Wang, *J. Power Sources*, 2009, **190**, 578.

37. S. S. Moganty, R. E. Baltus and D. Roy, *Chem. Phys. Lett.*, 2009, **483**, 90.

38. E. Song, and J. W. Choi, *Nanomaterials*, 2013, **3**, 498.

39. Z. L. Wang, X. J. He, S. H. Ye, Y. X. Tong, and G. R. Li, *ACS Appl. Mater. Interfaces*, 2014, **6**, 642.

40. K. Pandey, P. Yadav and I. Mukhopadhyay, *J. Solid State Electrochem.*, 2014, **18**, 453.

41. W. Sugimoto, H. Iwata, K. Yokoshima, Y. Murakami, and Y. Takasu, *J. Phys. Chem. B*, 2005, **109**, 7330.

42. H. Farsi, F. Gobal, H. Raissi and S. Moghiminia, *J. Solid State Electrochem.*, 2010, **14**, 643.

43. J. Bisquert, *Phys. Chem. Chem. Phys.,* 2007, **10**, 49.

44. C. Masarapu , H. F. Zeng , K. H. Hung and B. Wei, *ACS Nano*, 2009, **3**, 2199.

45. A. B. Afzal, M. J. Akhtar, M. Nadeem and M. M. Hassan, *Curr. Appl. Phys.* 2010, **10**, 601.

46. C. Yang, M. Zhou and Q. Xu, *Phys. Chem. Chem. Phys.*, 2013, **15**, 19730.